Journal of Hazardous Materials 166 (2009) 860–865

Contents lists available at ScienceDirect

Journal of Hazardous Materials

journal homepage: www.elsevier.com/locate/jhazmat

Environmentally friendly efficient coupling of *n*-heptane by sulfated tri-component metal oxides in slurry bubble column reactor

Hongzhu Ma*, Jing Xiao, Bo Wang

Institute of Energy Chemistry, School of Chemistry and Materials Science, Shaanxi Normal University, Xi'An 710062, PR China

ARTICLE INFO

Article history:
Received 25 May 2008
Received in revised form
26 September 2008
Accepted 26 November 2008
Available online 3 December 2008

Keywords:
Sulfated metal oxides
Slurry bubble column reactors
Cetane number
n-heptane
Long linear alkane

ABSTRACT

SO_4^{2-}/M_xO_y is of the greatest interest in solid catalysts and green catalysts. Slurry bubble column reactors are of considerable interest in industrial processes and various biochemical processes. The cetane number (CN) has widely used diesel fuel quality parameter related to the ignition delay time (and combustion quality) of a fuel. CN improvement of diesel fuels is a difficult task that refiners will face in the near future. For that purpose, the tests were designed in which *n*-heptane is used as the reactant in the air or ozone atmosphere at room temperature (RT) and local atmospheric pressure (LAP) using different catalysts of sulfated tri-component metal oxides SO_4^{2-}/Fe_2O_3-TiO_2-SnO_2 (SFTSn) and SO_4^{2-}/MnO_2-TiO_2-SnO_2 (SMTSn) in slurry bubble column reactor. The products distribution was analyzed by gas chromatography–mass spectrometry (GC–MS) method and the results show that the relative selectivity of long linear alkane (C_{12}–C_{28}) reaches the maximum (87.330%) when SMTSn is used as catalyst in flow air at 60 min. Diesel fuel components with higher cetane numbers can be easily obtained from this study.

1. Introduction

SO_4^{2-}/M_xO_y is a new type of catalyst; it has some advantages such as it has good acid strength, it is quite stable to moisture, air and heat, is easily separated, less corrosive to reactors and containers, and more friendly to the environment [1]. So it has been extensively used in many organic catalytic reactions of esterification, isomerization of *n*-alkanes, polymerization, acylation, and so on [2]. It can be said that sulfated metal oxides are the most important environmentally friendly heterogeneous catalysts to substitute current liquid acids and halogen-based solid acids, with increasing emphasis on green chemistry [3].

Slurry bubble column reactors (SBCRs) are cylindrical vessels in which gas is sparged into a suspension of liquid and fine solids (typically catalyst). These reactors are of considerable interest in industrial processes such as oxidation, hydrogenation of heavy oils, Fischer–Tropsch synthesis, liquid phase methanol synthesis, chlorination, alkylation, wastewater treatment, and various biochemical processes [4]. Their advantages include low pressure drop in the reactor, excellent heat transfer characteristics resulting in stable reactor temperatures, no diffusion limitations, and possibility of continuous refreshment of catalyst particles [5].

Recent environmental legislation on diesel fuel, which is a fuel derived from petroleum and consists mainly of aliphatics containing 8–28 carbon atoms, with ebullition points varying from 460 to 690 K [6], focuses on sulfur content, polynuclear aromatics (PNA), and cetane number (CN) [7]. The cetane number, dependent upon the chemical composition of diesel fuel, is a dimensionless descriptor for the ignition delay (ID) time of a diesel fuel upon injection into the combustion chamber [8]. Diesel fuel with a high CN has a short ignition delay period and starts to combust shortly after it is injected into an engine where air has been compressed and, consequently, heated to a high temperature. While the ignition delay can be influenced by the engine type and operating conditions.

Generally speaking, normal paraffins have high CN that increases with molecular weight. At the same carbon number, isoparaffins have lower CN than *n*-paraffins. Also, iso- and cyclo-paraffin have lower CNs than those with one long linear chain with the same carbon [9]. Therefore, several approaches have been proposed for the improvement of CN about diesel fuel to meet environmental legislation regulations. One approach is to use compounds known as "cetane boosters" to improve CN, but it will increase the flammability of the fuel which are potentially more hazardous. Another simple and effective method is directly transforming cyclo-paraffin into linear paraffin.

As an option to reach a higher CN, while simultaneously reducing aromatics, is further upgrading the petroleum stream by deep hydrotreating. The resulting CN greatly depends upon the nature of the crude as well as the refinery blending strategies. Even after deep hydrogenation, the expected high CN regulations may not be met.

Some researchers have suggested that chain polymerization process is a potential solution for significantly improving CN [10–12]. The main aim of this work is to study the feasibility of syn-

* Corresponding author. Tel.: +86 29 85308442; fax: +86 29 85307774.
E-mail address: wangbo@snnu.edu.cn (H. Ma).

0304-3894/$ – see front matter © 2008 Elsevier B.V. All rights reserved.
doi:10.1016/j.jhazmat.2008.11.096

thesis of linear long chain paraffin from low weight alkanes directly at room temperature (RT) and local atmospheric pressure (LAP).

To exemplify the approach, some tests have been selected: *n*-heptane coupling at room temperature and local atmospheric pressure catalyzed by sulfated tri-component metal oxides of SO_4^{2-}/Fe_2O_3-TiO_2-SnO_2 (SFTSn) and SO_4^{2-}/MnO_2-TiO_2-SnO_2 (SMTSn) in slurry bubble column reactor. The catalyst was characterized by means of Thermogravimetric-Differential scanning calorimetry (TG-DSC), X-ray photoelectron spectroscopy (XPS), Fourier transform infrared spectroscopy (FT-IR), and X-ray diffraction (XRD). The distributions of the products were investigated by gas chromatography–mass spectrometry (GC–MS), and the results show that the main products are the C number of *n*-alkane from C_{12} to C_{28}, which can all be used as diesel fuel components that have higher cetane numbers.

2. Experimental

2.1. Sulfated metal oxides preparation

The reactants and solvents used were of analytical grade and used without any further purification. $FeCl_3$, $MnSO_4{\cdot}H_2O$, $SnCl_4{\cdot}5H_2O$, $TiCl_4$, H_2SO_4 (98%), $NH_3{\cdot}H_2O$ (25–28%) and *n*-heptane were obtained from Xi'an Reagent Co.

The sulfated metal oxides were prepared by adopting a two-step route [13]. The metal precursors were prepared by a homogeneous co-precipitation method [14]. For this purpose, an aqueous solution containing the requisite quantities of $FeCl_3$, $TiCl_4$ and $SnCl_4$, and the other aqueous solution containing the requisite quantities of $MnSO_4$, $TiCl_4$ and $SnCl_4$ were prepared and mixed together separately. The solutions were hydrolyzed with ammonium hydroxide (25%) with vigorous stirring until the pH of the solution reached to 8–9, and then mixed precipitates were formed and allowed to settle for 24 h. The precipitates were filtrated off and extensively washed with deionized water, and dried at 373 K for 12 h. Then, sulfation of the amorphous hydroxides was carried out by the following procedure: treatment with sulfuric acid (0.5 M) (5 ml of acid solution per 1 g of solid) at room temperature for 6 h, followed by filtration and drying at 373 K for 3 h. Finally, all the samples were calcined at temperature 873 K for 3 h to obtain the sulfated tri-component metal oxides SO_4^{2-}/Fe_2O_3-TiO_2-SnO_2 (SFTSn) and SO_4^{2-}/MnO_2-TiO_2-SnO_2 (SMTSn).

2.2. Experimental set-up and analysis of the products

Fig. 1 shows the schematic diagram of experimental set-up for catalytic reaction. The reactor system mainly comprises a reactor. At room temperature and normal atmospheric pressure, to make the gas–liquid–solid three phases contacted sufficiently, slurry bubble column reactor was used, which contained 120 ml *n*-heptane and 10 g catalyst, and the oxidant was continuously input by a gas generator. The reaction cell was cooled by the cooling water in a trough to form the room temperature condition, and the reactor system was airproofed to prevent the volatilization of organic compound. The compositions of reaction mixture were identified with gas chromatography (GC) (Agilent 6890)–mass spectrometry (MS) (5973, Hewlett-Packard, Palo Alto, CA, USA). The GC–MS condition was as follows: Helium carrier gas with 1.00 ml/min of flow rate was used. The oven temperature was programmed from 323 to 533 K. The effluent from GC column was directly connected to MS.

2.3. Characterization of the catalyst

Thermal analysis (TG-DSC) of the uncalcined samples was performed on a Q1000DSC + LNCS + FACS Q600SDT thermoanalyzer (TA Co., USA), under air atmosphere, in the temperature range 25–1000 °C with a heating velocity rate of 10 °C/min.

The presence of sulfate groups in the samples was confirmed using a FI-IR Equinx55 model (Brucher Co., Ettlingen, Germany) spectrum equipment, in the range of 400–4000 cm^{-1}. The samples were prepared as potassium bromide discs, in a 1:100 proportion.

The XPS spectra were acquired with a XSAM800 (Kratos) equipment, with source of X-rays, Mg Kα (1253.6 eV) anode and 4000 W power and hemispheric electron analyzer. The base pressure in the chamber was in the range of 10^{-8} Pa. This reference was in all cases in good agreement with the binding energy (BE) of the C 1s peak, arising from contamination, at 284.6 eV.

The XRD powder patterns of the solid were recorded on a D/Max2550VB diffractometer (Rigaku D/Max2550VB + /PC, Kawazaki, Japan) using Cu Kα radiation (λ = 0.15406 nm), at 40 kV and 40 mA with scan speed 8 °/min in a 2θ (10–70°) and at a rate of 0.02 °/s.

3. Results and discussion

3.1. Thermoanalysis

DSC can easily differentiate between physically and chemically adsorbed phases through the thermogram as endothermic and exothermic transition peaks, respectively [15]. The DSC–TG results of the uncalcined samples are shown in Figs. 2 and 3, respectively. Below 250 °C two endothermic peaks observed can be attributed to the removal of water (in hydration or structural). In the region

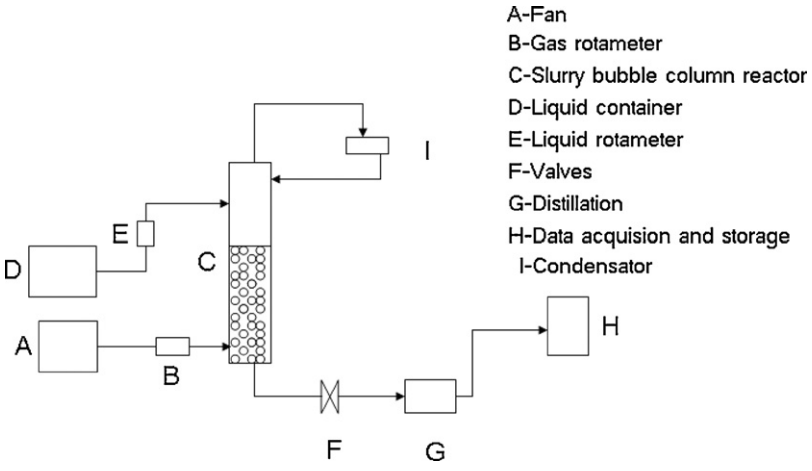

Fig. 1. The schematic diagram of experimental set-up.

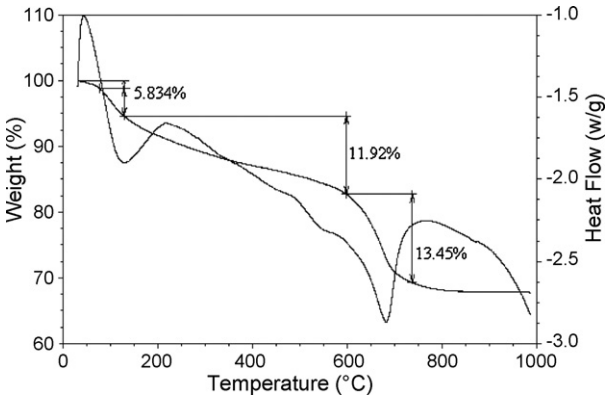

Fig. 2. DSC–TG of the uncalcined SFTSn.

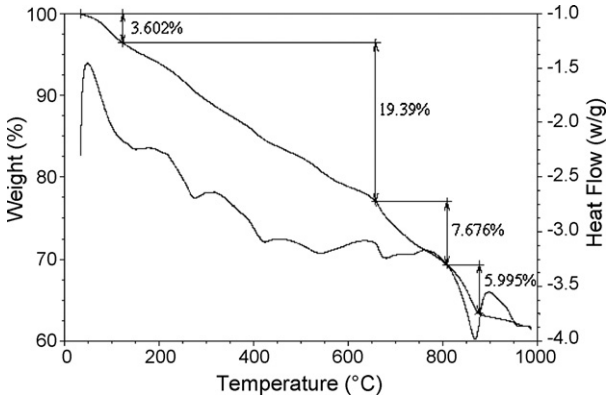

Fig. 3. DSC–TG of the uncalcined SMTSn.

of 300–600 °C, there is a loss of mass and some endothermic and exothermic transition peaks, which can be due to the effect of phase transformation and oxide valence change. And a loss of mass was observed at 650–900 °C which might be the result of the crystallization of the sample and the evolution of SO_3 decomposed from the sulfate species bonded to the surface of the sample. The presence of distinct regions of sulfate loss have already been reported in studies by Ward and Ko [16], who prepared sulfated ZrO_2 with high and low sulfate contents.

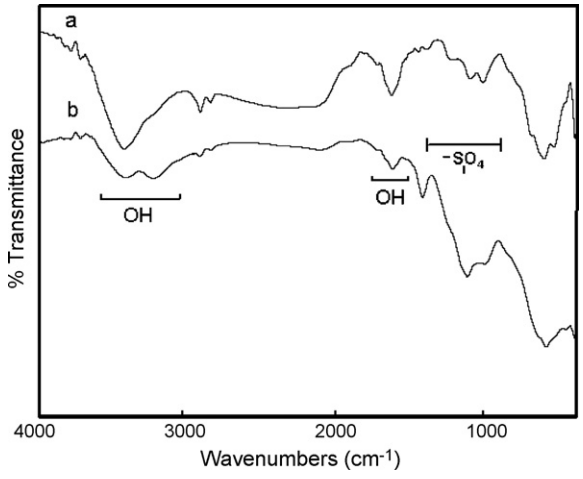

Fig. 4. FT-IR spectra of different catalysts before reaction [(a) SFTSn catalyst; (b) SMTSn catalyst].

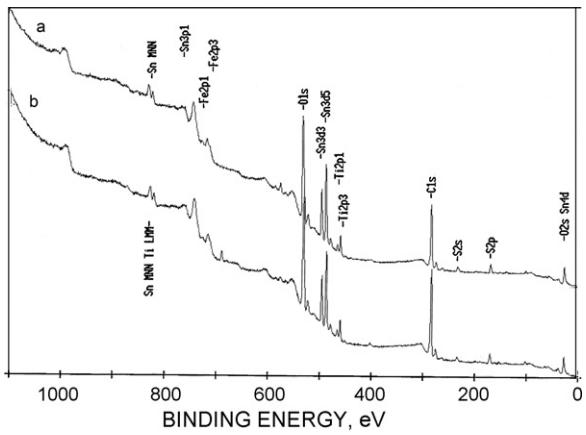

Fig. 5. XPS of SFTSn before (b) and after (a) the reaction.

3.2. FT–IR spectroscopy

The IR spectrum of SFTSn and SMTSn before the reaction shows a huge band with a maximum at around 3500 cm^{-1} in the OH stretching region (Fig. 4), which was can be attributed to hydroxyls groups coordinated to metal cation [17,18] or the band of H_2O molecule. Additionally, in Fig. 4a, a shoulder band at around 3200 cm^{-1} can be assigned to terminal Mn–OH^{2+} groups, where the OH were combined with protons creating a new type of acid sites, or to OH groups strongly interacting with each other or with the surface through hydrogen bond [19]. The band at about 1632 cm^{-1} is assigned to the deformation vibration mode of the adsorbed water in the sulfated metal oxides [20], indicating that the sulfated metal oxides was not completely dehydrated during activation.

In general, when metal oxides were modified with sulfate ion followed by evacuating above 400 °C, a strong band assigned to S=O stretching frequency was observed at 1360–1410 cm^{-1} [21–26]. In the figure, obvious bands observed at around 1400 and 1100 cm^{-1}, assigned to the asymmetric stretching vibration and symmetric stretching vibration band of the O=S=O, respectively, indicated that a chelate bidentate SO_4^{2-} coordinated to metal oxides [21] because the highest stretching vibration of the SO_4^{2-} in the samples was above 1200 cm^{-1} [17,18]. It also maybe inferred that sulfur element in the sulfated metal oxides existed in a six-oxidation state (S^{6+}). These results were very similar to those reported by other authors [17,27,28].

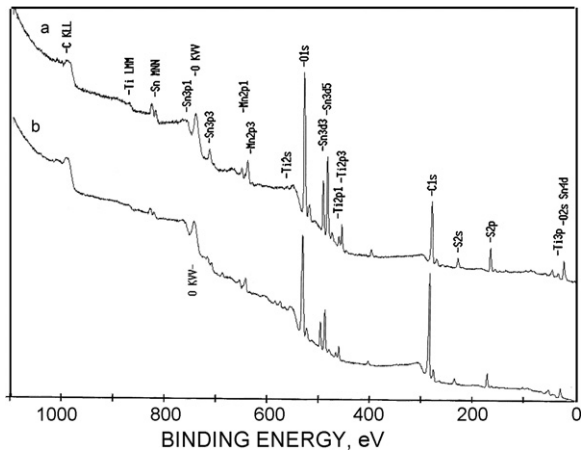

Fig. 6. XPS of SMTSn before (b) and after (a) the reaction.

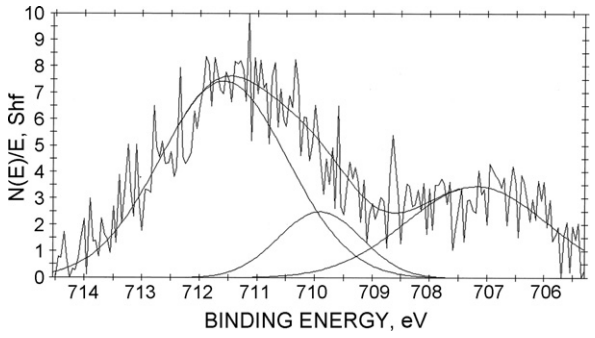

Fig. 7. Binding energy and valence simulation curve of Fe 2p3/2 in SFTSn after the reaction in air.

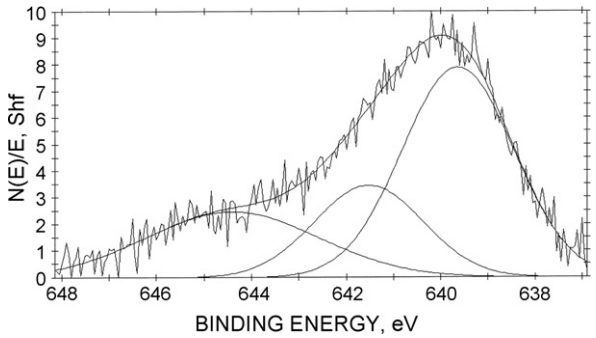

Fig. 8. Binding energy and valence simulation curve of Mn 2p3/2 in SMTSn after the reaction in ozone.

3.3. XPS

Before and after the reactions, binding energy of all the elements of the sulfated metal oxides (SFTSn and SMTSn) was shown in Figs. 5 and 6, respectively. The binding energy of sulfur S 2p was observed at 168.4 eV, agreed with these results that were reported by other authors [29–31], which suggested that sulfur in the sulfated metal oxides existed in a six-oxidation state (S^{6+}), which is also consistent with the result of FT–IR. After the reaction, the binding energies of S 2p were almost unchanged, inferring that the valence of S was unchanged, it may be concluded that the sulfated metal oxides can be reused and the catalytic activity was almost unchanged.

SFTSn and SMTSn samples showed similar Ti 3d5/2 and Sn 3d5/2 binding energy values around 458.5–458.3 eV and 486.6–486.9 eV, respectively, which suggested the presence of Ti^{4+} and Sn^{4+} in the samples, and it agrees well with the data reported in literatures [32,33]. But the elements of Fe and Mn had variable valence and Fig. 7 shows the deconvoluted Fe 2p3/2 XPS spectra after reaction in air. The different binding energies of 711.37, 709.44 and 706.27 eV assigned to three valent components Fe^{3+}, Fe^{2+} and Fe^{0}. Fig. 8 shows the deconvoluted Mn 2p3/2 XPS spectra after reaction in ozone, the different binding energies of 644.40, 641.53 and 639.64 eV assigned to three valent components Mn^{4+}, Mn^{3+} and Mn^{2+}, which illuminated that Fe and Mn species were involved in the coupling reaction.

3.4. XRD

Calcined SFTSn and SMTSn samples before and after the reactions were characterized by XRD. It can be seen from the XRD patterns (Fig. 9) that the main typical diffraction peaks characteristic of tetragonal SnO_2 (t-SnO_2) are observed for all samples, in agreement with previous literatures [34,35]. But XRD analysis does not obviously present any characteristic diffraction peaks of titanium oxide, iron oxide and manganese oxide. Therefore, titanium oxide, iron oxide and manganese oxide would be either amorphous or very well dispersed on the SnO_2 phase. And there are no characteristic peaks of metal sulphate in the patterns. There are little differences in XRD patterns before and after reaction, maybe indicating that no changes in the phase occurred in the process of the reaction. It can be concluded that the structures of the samples are very stable during the reaction.

3.5. GC–MS analysis

The product distribution was taken for GC–MS analysis, which was known for its superior separation of complex organic com-

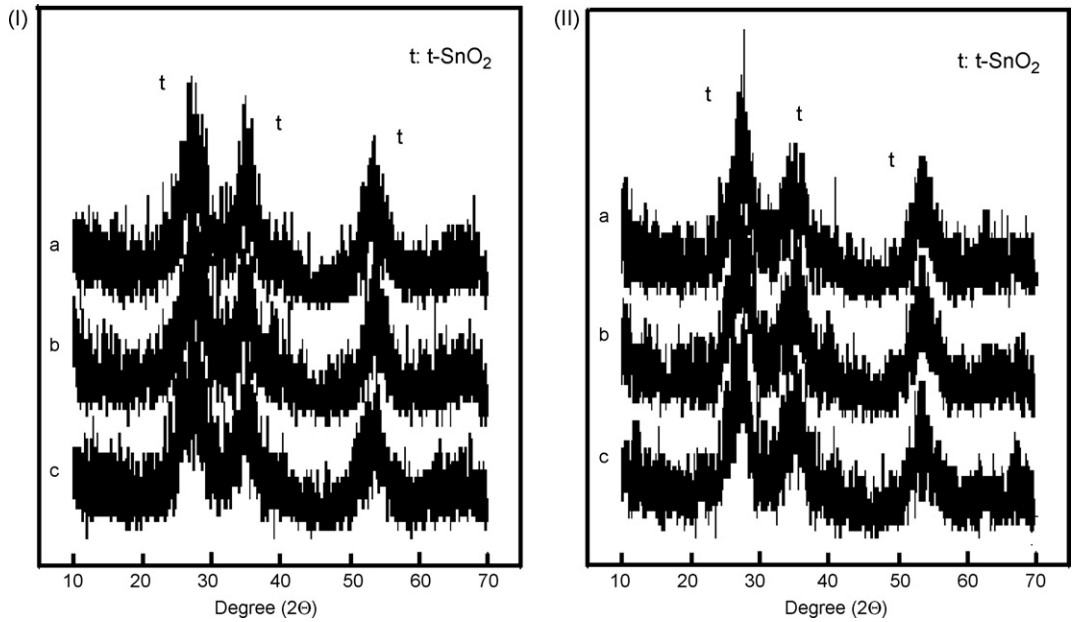

Fig. 9. X-ray diffraction patterns of different catalysts [(I) SFTSn; (II) SMTSn] before and after the reaction [(a) before the reaction; (b) after the reaction in air; (c) after the reaction in ozone].

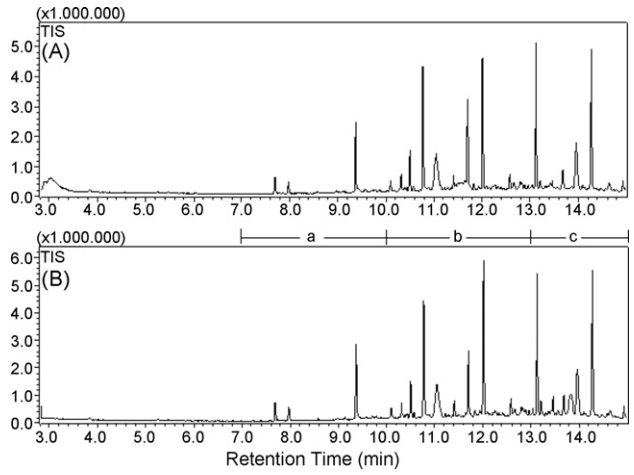

Fig. 10. The GC of the products reacted using SFTSn in flow air [(a) at 30 min; (b) at 60 min].

pounds, greater sensitivity, and shorter measuring time [36]. The effluent from GC column was directly connected to MS. The main peaks on GC patterns were identified by comparing their mass spectra with NIST library data and the result was verified by comparing retention time of the product with that of the standards. The effect of various factors in the process of the coupling of *n*-heptane was investigated by the product analysis.

(1) Time factor: Fig. 10 showed the total ion chromatogram (TIC) of the products (the peak of the solvent was taken off) at 30 and 60 min using SFTSn in flow air. The relative selectivity of different products at different times (30, 60 and 90 min) under the same reaction condition was shown in Table 1. GC data of every product at 30 min presented that no docosane (retention time: 13.82 min) appeared but it obviously appeared at 60 min, however, others remained almost unchanged and the relative selectivity of main products is very similar as Table 1 shows. Compared with these GC data, the conversion of *n*-heptane was different and reached the maximum at 60 min by qualitative analysis from the TIC. The results show that reaction time has some effect on the reaction and 60 min has been selected as the optimal reaction time.

Table 1
Distribution of the products of the coupling reaction using SFTSn in flow air at different time.

No.	Linear alkanes (C_n–C_m)	Relative selectivity (%)		
		30 min	60 min	90 min
a	C_{12}–C_{14}	7.644	7.146	6.872
b	C_{15}–C_{20}	36.677	32.197	34.935
c	C_{21}–C_{28}	40.426	47.906	44.250
a + b + c	C_{12}–C_{28}	84.747	87.249	86.057

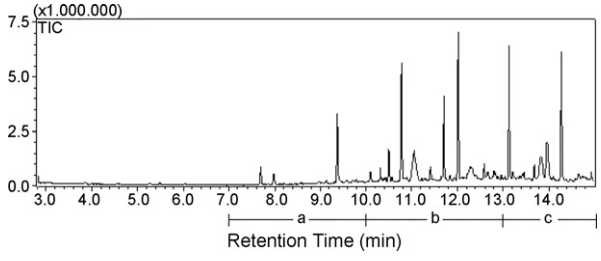

Fig. 11. The GC of the products reacted using SMTSn in flow air at 60 min.

Table 2
Distribution of the products of the coupling reaction using different catalysts in flow air at 60 min.

No.	Linear alkanes (C_n–C_m)	Relative selectivity (%)	
		SFTSn	SMTSn
a	C_{12}–C_{14}	7.146	7.056
b	C_{15}–C_{20}	32.197	33.291
c	C_{21}–C_{28}	47.906	46.983
a + b + c	C_{12}–C_{28}	87.249	87.330

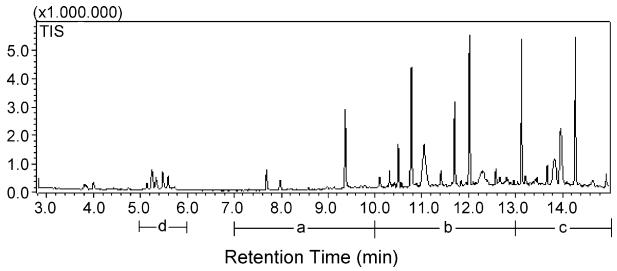

Fig. 12. The GC of the products reacted using SFTSn in flow ozone at 60 min.

(2) Sulfated metal oxides factor: Fig. 11 showed the TIC of the products (the peak of the solvent was taken off) at 60 min using SMTSn in flow air. The relative selectivity of different products using different sulfated metal oxides under the above reaction condition was shown in Table 2. Comparing with Fig. 10b, the products were the same and their relative selectivity was similar (Table 2), but the conversion of *n*-heptane was higher with SMTSn than that of SFTSn by qualitative analysis from the TIC.
(3) Oxidant factor: Fig. 12 showed the TIC of the products (the peak of the solvent was taken off) at 60 min using SFTSn in flow ozone. The relative selectivity of different products using different oxidant under above reaction condition was shown in Table 3. There were some difference between Figs. 12 and 10b: some new products (retention time: 5.17–5.60 min) appear in Fig. 12, oxygenous ramifications (heptan-4-ol, heptan-2-ol, 2-methylhexan-3-ol, heptan-3-one and 4-methylhexan-2-one), and their total relative selectivity is rather high (6.635%). The relative selectivity of long linear alkane (C_{12}–C_{28}) decreased in flow ozone using the identical sulfated metal oxides at the same reaction time.

To sum up, the above-mentioned three factors have some effect on the reaction process of the coupling of *n*-heptane. Long linear alkane could be obtained from one-pot environmentally friendly efficient coupling of *n*-heptane by SFTSn or SMTSn in the air or ozone atmosphere at RT and LAP. Moreover, the relative selectivity (87.330%) of long linear alkane (C_{12}–C_{28}) from *n*-heptane reaches the maximum when the reaction under SMTSn catalyst in flow air at 60 min is a little higher than that of reference reported (83.785%) [37].

Table 3
Distribution of the products of the coupling reaction using SFTSn in different oxidant at 60 min.

No.	Main product	Relative selectivity (%)	
		Air	Ozone
a	C_{12}–C_{14}	7.146	6.288
b	C_{15}–C_{20}	32.197	32.971
c	C_{21}–C_{28}	47.906	42.255
d	Oxygenous ramifications	–	6.635
a + b + c	C_{12}–C_{28}	87.249	81.514

4. Conclusion

The sulfated metal oxides samples were characterized by TG-DSC, FI-IR, XPS, and XRD techniques, which indicated that a chelate bidentate SO_4^{2-} coordinated to metal oxides. In the tests, *n*-heptane was as the reactant in the air or ozone atmosphere under RT and LAP using different sulfured tri-component metal oxides (SFTSn and SMTSn) in slurry bubble column reactor. And the compositions of reaction mixture were identified with GC–MS. The reaction result portrayed that the diesel oil fractions (C_{12}–C_{28}) with high CN could be gotten by one-pot environmentally friendly efficient coupling of *n*-heptane under above condition. The highest selectivity of C_{12}–C_{28} in the reactions was 87.330%.

References

[1] T. Yamaguchi, Recent progress in solid superacid, Appl. Catal. 61 (1990) 1–25.
[2] B.M. Reddy, P.M. Sreekanth, V.R. Reddy, Modified zirconia solid acid catalysts for organic synthesis and transformations, J. Mol. Catal. 225 (2005) 71–78.
[3] P.T. Anastas, J.J. Breen, Design for the environment and green chemistry: the heart and soul of industrial ecology, J. Cleaner Prod. 5 (1997) 97–102.
[4] N. Rados, A. Shaikh, M.H. Al-Dahhan, Solids flowmapping in a high pressure slurry bubble column, Chem. Eng. Sci. 60 (2005) 6067–6072.
[5] V.A.P. O'Shea, M.C. Álvarez-Galván, J.M. Campos-Martín, J.L.G. Fierro, Fischer–Tropsch synthesis on mono- and bimetallic Co and Fe catalysts in fixed-bed and slurry reactors, Appl. Catal. A: Gen. 326 (2007) 65–73.
[6] D.J. Cookson, B.E. Smith, Observed and predicted properties of jet and diesel fuels formulated from coal liquefaction and Fischer–Tropsch feedstocks, Energy Fuels 6 (1992) 581–585.
[7] C.S. Roberto, T.D. Phuong, S. Malee, E.A. Walter, D.T. Joshua, L.S. Edward, E.R. Daniel, Evaluation of different reaction strategies for the improvement of cetane number in diesel fuels, Fuel 85 (2006) 643–656.
[8] K. Gerhard, C.M. Andrew, W.R. Thomas, Cetane numbers of branched and straight-chain fatty esters determined in an ignition quality tester, Fuel 82 (2003) 971–975.
[9] H. Yang, Z. Ring, Y. Briker, N. McLean, W. Friesen, C. Fairbridge, Neural network prediction of cetane number and density of diesel fuel from its chemical composition determined by LC and GC–MS, Fuel 81 (2002) 65–74.
[10] R.C. Santana, P.T. Do, M. Santikunaporn, W.E. Alvarez, J.D. Taylor, E.L. Sughrue, D.E. Resasco, Evaluation of different reaction strategies for the improvement of cetane number in diesel fuels, Fuel 85 (2006) 643–656.
[11] A.S. Ramadhas, S. Jayaraj, C. Muraleedharan, K. Padmakumari, Artificial neural networks used for the prediction of the cetane number of biodiesel, Energy 31 (2006) 2524–2533.
[12] X.C. Lu, J.G. Yang, W.G. Zhang, Z. Huang, Improving the combustion and emissions of direct injection compression ignition engines using oxygenated fuel additives combined with a cetane number improver, Energy Fuels 19 (2005) 1879–1888.
[13] J. Pasel, V. Speer, C. Albrecht, F. Richter, H. Papp, Metal doped sulfated ZrO2 as catalyst for the selective catalytic reduction (SCR) of NO with propane, Appl. Catal. B: Environ. 25 (2000) 105–113.
[14] G. Lu, Catalytic properties of SO_4^{2-}/Ti-M-O superacids in esterification, Appl. Catal. A: Gen. 133 (1995) 11–18.
[15] A. Aboul-Gheit, Acid site strength distribution in mordenites by differential scanning calorimetry, J. Catal. 113 (1988) 490–496.
[16] D.A. Ward, E.I. Ko, One-step synthesis and characterization of zirconia-sulfate aerogels as solid superacids, J. Catal. 150 (1994) 18–33.
[17] H. Ma, J. Li, B. Wang, Esterification and polymerization by catalytic oxidation of cyclohexane at room temperature over modified sulfated TiO_2 in the air, Energy Fuel 21 (2007) 1859–1862.
[18] K. Fottinger, G. Kinger, H. Vinek, In situ IR investigation of *n*-hexane isomerization over Pt containing sulfated zirconia, Appl. Catal. A: Gen. 266 (2004) 195–202.
[19] J.A. Moreno, G. Poncelet, Isomerization of *n*-butane over sulfated Al- and Ga-promoted zirconium oxide catalysts influence of promoter and preparation method, J. Catal. 203 (2001) 453–465.
[20] A. Bellifa, D. Lahcene, Y.N. Tchenar, A. Choukchou-Braham, R. Bachir, S. Bedrane, C. Kappenstein, Preparation and characterization of 20 wt.% V2O5–TiO2 catalyst oxidation of cyclohexane, Appl. Catal. A: Gen. 305 (2006) 1–6.
[21] J.R. Sohn, J.G. Kin, T.V. Kwon, E.H. Park, Measurement of the thermal properties of gadolinium and dysprosium titanate, Langmuir 18 (2002) 1666–1673.
[22] O. Sanur, M. Bensitel, A.B.M. Saad, J.C. Cavallcy, C.P. Tripp, B.A. Morrow, The structure and stability of sulfated alumina and titania, J. Catal. 99 (1986) 104–110.
[23] T. Yamaguchi, Recent progress in solid superacid, Appl. Catal. 61 (1990) 1–11.
[24] H. Matsuhashi, H. Shibata, H. Nakamura, K. Arata, Skeletal isomerization mechanism of alkanes over solid superacid of sulfated zirconia, Appl. Catal. A: Gen. 187 (1999) 99–106.
[25] A. Corma, H. Garcia, Naphthalene included within all-silica zeolites: influence of the host on the naphthalene photophysics, Chem. Rev. 102 (2002) 3837–3849.
[26] B. Moden, Bi-ZengZhan, J. Dakka, J.G. Santiesteban, E. Iglesia, Kinetics and mechanism of cyclohexane oxidation on MnAPO-5 catalysts, J. Catal. 239 (2006) 390–401.
[27] K. Fottinger, E. Halwax, H. Vinek, Deactivation and regeneration of Pt containing sulfated zirconia and sulfated zirconia, Appl. Catal. A: Gen. 301 (2006) 115–122.
[28] S.M. Jung, P. Grange, Characterization and reactivity of pure TiO_2–SO_4^{2-} SCR catalyst: influence of SO_4^{2-} content, Catal. Today 59 (2000) 305–312.
[29] B.M. Reddya, P.M. Sreekanth, Y. Yamadab, Q. Xub, T. Kobayashi, Surface characterization of sulfate, molybdate, and tungstate promoted TiO_2–ZrO_2 solid acid catalysts by XPS and other techniques, Appl. Catal. A: Gen. 228 (2002) 269–278.
[30] B.M. Reddya, P.M. Sreekantha, Y. Yamada, T. Kobayashib, Surface characterization and catalytic activity of sulfate-, molybdate- and tungstatepromoted Al_2O_3–ZrO_2 solid acid catalysts, J. Mol. Catal. A: Chem. 227 (2005) 81–89.
[31] L.M. Martınez, T.C. Montesdecorrea, J.A. Odriozola, M.A. Centeno, Synthesis and characterization of sol–gel zirconia supported Pd and Ni catalysts, Catal. Today 107 (2005) 800–808.
[32] J.P. Chen, R.T. Yang, Selective catalytic reduction of NO with NH_3 on $SO^{-2}{}_4/TiO_2$ superacid catalyst, J. Catal. 139 (1993) 277–288.
[33] J.Ph. Nogier, M. Delamar, Chapter 7.1 X-ray photoelectron spectroscopy of TiO_2/V_2O_5 catalysts, Catal. Today 20 (1994) 109–123.
[34] P. Salas, J.G. Hernhndez, J.A. Montoya, J. Navarrete, J. Salmones, Effect of tin content on silica mixed oxides: sulfated and unsulfated catalysts, J. Mol. Catal. A: Chem. 123 (1997) 149–154.
[35] N. Nava, P.D. Angel, J. Salmones, E. Baggio-Saitovitch, P. Santiago, Tin-Platinum catalysts interactions on titania and silica, Appl. Surf. Sci. 253 (2007) 9215–9220.
[36] A.G. Giumanini, G. Verardo, Identification of mononitro and dinitro isomers of diphenylmethane by GC–FT–IR and GC–MS techniques, Ind. Eng. Chem. Res. 40 (2001) 1449–1453.
[37] B. Wang, X. Cui, H. Ma, J. Li, Photocatalytic activity of SO_4^{2-}/SnO_2-TiO_2 catalysts: direct oxidation of *n*-heptane to ester under mild conditions, Energy Fuels 21 (2007) 3748–3749.